engineering proceedings

MDPI

Proceeding Paper

The Effect of Weaving Pattern on the Material Characteristics of the Textile Composite Layer †

Gergely Bojtár

Department of Applied Mechanics, AUDI Hungaria Faculty of Engineering, Széchenyi István University, Egyetem tér 1, H-9026 Győr, Hungary; bojtar@sze.hu

† Presented at the Sustainable Mobility and Transportation Symposium 2026, Győr, Hungary, 8 October 2026.

Abstract

The article demonstrates how textile weave patterns influence the orthotropic material properties of a textile composite layer. The examined textiles have two mutually perpendicular fiber directions. The density of the longitudinal and transverse fiber bundles is the same in the layer models. In the fabric, the warp and weft fiber bundles alternately pass over and under each other. This study investigates how the material properties of a textile composite layer change when the waviness of the fiber bundles varies over a given length. There are different weaving patterns in the finite element layer models. The fiber bundle passes over or under several consecutive perpendicular fiber bundles. The volume fraction of the textile in the composite layer is only slightly affected by the waviness of the fiber bundles. As a result of tensile loading, the waviness of the rovings decreases in the loading direction and increases in the perpendicular direction.

Keywords: composite; textile weave pattern; orthotropic material properties; finite element method

1. Introduction

Laminated textile composite plates consist of a single layer of flat woven fabric in each ply. Within the fabric, the elementary reinforcing fibers are grouped into fiber bundles, known as rovings, which may be either untwisted or twisted. In an untwisted roving, the elementary fibers are aligned parallel to one another, whereas in a twisted roving they follow a helical arrangement. Most textile reinforcements have two mutually perpendicular fiber directions. The fabric is formed by the regular interlacing of warp and weft rovings, which are oriented perpendicular to each other.

There are many well-known methods of weaving warp and weft fabrics. However, all of them can be traced back to three basic weave patterns and their variations [1]. The three fundamental weaves are shown in Figure 1: (a) plain weave, (b) twill weave, and (c) satin weave. In Figure 1, the warp yarns are shown in gray, while the weft yarns are shown in white. In addition to woven fabrics, there are also nonwoven, non-crimp, stitched, and knitted fabrics. Owing to their fiber architecture, these materials exhibit optimized strength properties. An example is shown in Figure 2 [2].

The mechanical behavior of a composite layer is also influenced by the geometry of the textile reinforcement. According to the construction report [2], the strength of plain-woven fabrics is reduced by the waviness of the rovings. Fibers provide their highest strength when they remain straight. Consequently, the mechanical properties of plain-woven textiles are relatively lower than those of many other weave types. In a plain weave, the rovings follow

Check for updates

Academic Editors: Gábor Dogossy, Szabolcs Kocsis-Szürke, Dániel Csikor, Dániel Serfőző, Miklós Kuczmann, András Lajos Nagy, László Lendvai and Ambrus Zelei

Published: 13 November 2026

Copyright: © 2026 by the author. Licensee MDPI, Basel, Switzerland. This article is an open access article distributed under the terms and conditions of the Creative Commons Attribution (CC BY) license.

a simple over-under pattern, passing alternately over and under adjacent rovings. The goal of my research is to determine how the mechanical properties of a textile-reinforced composite layer change when the rovings pass alternately over and under not just one, but multiple perpendicular rovings, so there are fewer waves in the textile reinforcement within a given area.

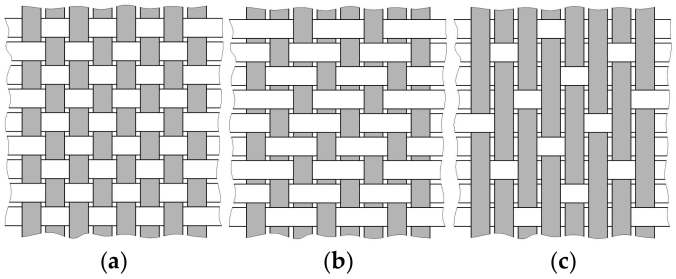


Figure 1. Basic 2D weaves: (**a**) Plain weave; (**b**) Twill weave; (**c**) Satin weave.

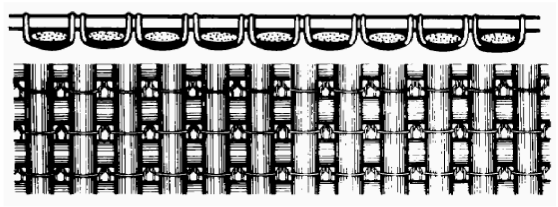


Figure 2. Knitted biaxial fabric.

2. Linear Elastic, Orthotropic Material Law

If the long reinforcing fibers in the material are oriented perpendicular to one another in the x_1 and x_2 directions, as shown in Figure 3, the material exhibits orthotropic behavior. Figure 3 illustrates the $x_1x_2x_3$ material coordinate system of the textile composite plate, where the x_1 axis corresponds to the warp direction of the textile, referred to as the longitudinal direction, and the x_2 corresponds to the weft direction, referred to as the transverse direction.

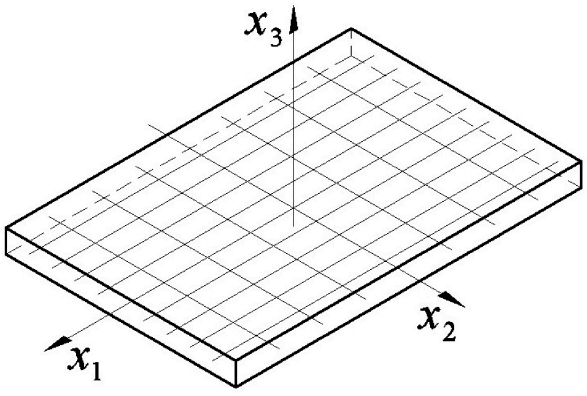


Figure 3. The principal material directions of the textile composite layer.

The material structure of the composite is heterogeneous. Each layer consists of matrix-impregnated textile reinforcement and matrix material. The behavior of such a textile composite layer can be described using a macroscopic orthotropic material model. Under

https://doi.org/10.3390/engproc2026157070

generalized plane stress conditions, the linear elastic orthotropic constitutive law in the material coordinate system of the layer can be expressed as follows [3–5]:

$$\begin{bmatrix} \overline{\varepsilon}_1 \\ \overline{\varepsilon}_2 \\ \overline{\gamma}_{12} \end{bmatrix} = \begin{bmatrix} \frac{1}{E_1} & -\frac{\nu_{21}}{E_2} & 0 \\ -\frac{\nu_{12}}{E_1} & \frac{1}{E_2} & 0 \\ 0 & 0 & \frac{1}{G_{12}} \end{bmatrix} \cdot \begin{bmatrix} \overline{\sigma}_1 \\ \overline{\sigma}_2 \\ \overline{\tau}_{12} \end{bmatrix}. \tag{1}$$

The average strain and stress in a textile composite layer of volume V can be defined as follows [4,6–8]:

$$\overline{\varepsilon}_{ij} = \frac{1}{V} \int_{(V)} \varepsilon_{ij} dV, \tag{2}$$

$$\overline{\sigma}_{ij} = \frac{1}{V} \int_{(V)} \sigma_{ij} dV, \ (i,j = 1,2). \tag{3}$$

Five macroscopic material properties define the relationship between the homogenized stresses and strains: the elastic moduli E_1 and E_2, the Poisson's ratios ν_{12} and ν_{21}, and the shear modulus G_{12}. Four of these parameters are independent, since the following equation can be derived from energy considerations [3,4,9]:

$$\frac{\nu_{12}}{E_1} = \frac{\nu_{21}}{E_2}. \tag{4}$$

3. Material Properties of the Matrix and the Roving

In the textile composites under investigation, the micron-thin elementary carbon fibers are arranged in untwisted, flat rovings. The composite consists of linear-elastic, orthotropic, transversely isotropic carbon fiber bundles embedded in a polyester matrix. The roving type is Torayca T300-3K (Toray Carbon Fibers America, Inc., Santa Ana, CA, USA). The "3K" denotes that each roving contains 3000 elementary carbon fibers. The matrix is a polyester resin of type AROPOL M105TB (Ashland Finland Oy, Lahti, Finland), which is a linear-elastic, isotropic material. A textile composite plate was laminated for the research described by me et al. [10,11]. It was reinforced with a SIGRATEX KDL 8003 type plain weave carbon fabric (SGL Carbon GmbH, SGL Technologies GmbH, Meitingen, Germany). The type of the roving was Torayca T300-3K and the matrix was AROPOL M105TB. The Young's modulus of the matrix material (E_m) and its Poisson's ratio (ν_m) were determined experimentally in accordance with the ASTM D638-10 standard [12]: $E_m = 3677$ MPa, $\nu_m = 0.346$. The shear modulus of the matrix material (G_m) was calculated using Equation (5), which is valid for isotropic materials:

$$G_m = \frac{E_m}{2(1+\nu_m)} = 1365.9\text{MPa}. \tag{5}$$

The cross section and waviness of the roving were determined after lamination by using microscopic measurements. In Figure 4, $x_{f1}x_{f2}x_{f3}$ denotes the material coordinate system of the orthotropic, transversely isotropic carbon fiber, while $x_{r1}x_{r2}x_{r3}$ denotes the material coordinate system of the matrix-impregnated roving. The x_{r1} axis is parallel to the fibers. Figure 4a shows one periodic unit of the roving, while Figure 4b shows the roving with its entire cross section.

The macroscopic material constants of the roving were obtained with a finite element model in article [11]. The roving model is based on a periodic unit cell (Figure 4a). The results of the calculations are presented in Table 1. The matrix-impregnated roving is modeled as a linear-elastic, orthotropic, transversely isotropic material. The plane of isotropy is the $x_{r2}x_{r3}$ plane.

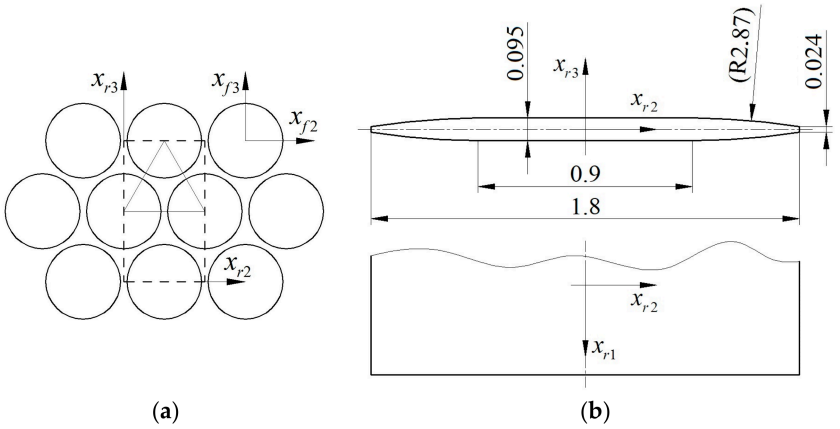


Figure 4. Matrix-impregnated roving: (**a**) One periodic unit within the roving; (**b**) Roving structure.

Table 1. Macroscopic material properties of the matrix-impregnated roving.

E_{r1} = 177,236 MPa	ν_{r12} = 0.202	G_{r12} = 4155 MPa
E_{r2} = 10,352 MPa	ν_{r23} = 0.430	G_{r23} = 3620 MPa
E_{r3} = 10,352 MPa	ν_{r13} = 0.202	G_{r13} = 4155 MPa

4. Finite Element Model-Cells

4.1. Examined Textile Reinforcements: Geometry of the Model-Cells

For comparability, the thickness of the composite layer, as well as the cross-section and spacing of the rovings in the x_1 and x_2 directions, are identical in all model-cells. These parameters are also shown in Figure 5. When the roving spacing is $t_1 = t_2 = 2$ mm, the roving density is $n_1 = n_2 = 5$ count/cm.

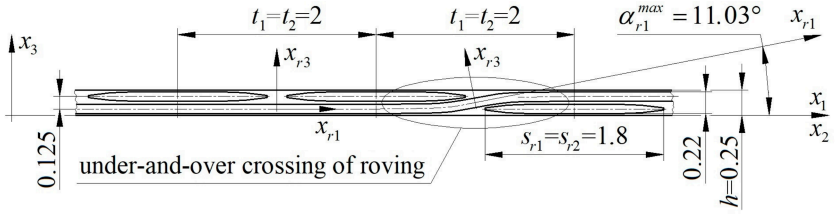


Figure 5. Reinforcing textile in the composite layer.

The principal material direction (x_{r1}) of the fiber bundle forms an angle α_{r1} with the x_1 and x_2 axes of the model-cell. This angle reaches its maximum absolute value at the inflection point of the half-wave, denoted as α_{r1}^{max}. The geometry of the under-and-over crossing is clearly characterized by the angle α_{r1}^{max} (Figure 5).

Basket weave is an extension and generalization of plain weave. A group of p warp rovings passes alternately under and over a group of q weft rovings (Figure 6). This is referred to as a $p \times q$ basket weave. A textile weaving unit consists of $2p$ warp rovings and $2q$ weft rovings. Four different textile-reinforced layers are modeled, as shown in Figure 6. The model-cells are indicated by dashed lines in the textile and each represents a symmetrical, periodic section. The plain-woven textile corresponds to a 1 × 1 basket weave (Figure 6a). I also examined a case without under-and-over interlacing. In the warp direction, a group contains $p = \infty$ rovings, and in the weft direction $q = \infty$ rovings. The $\infty \times \infty$ basket weave textile corresponds to a knitted biaxial fabric (Figure 6d). Such a fabric is also shown in Figure 2. Non-load-bearing fibers are not modeled.

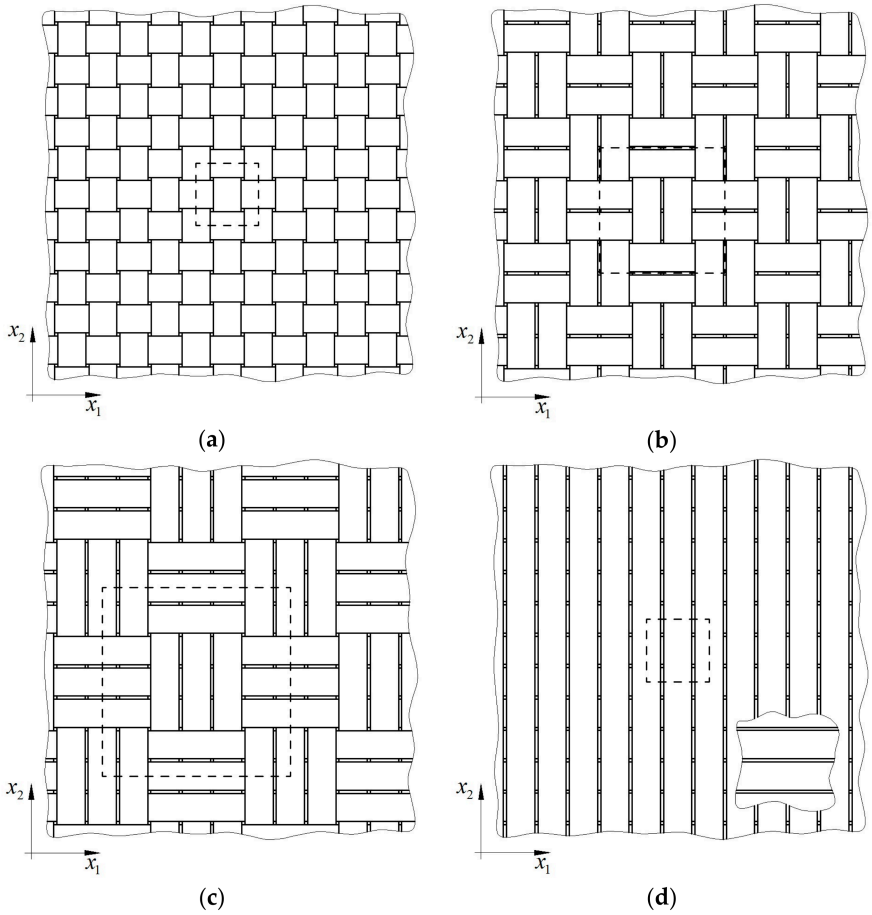


Figure 6. The textile reinforcements examined: (**a**) Plain weave textile (1 × 1); (**b**) 2 × 2 basket weave textile; (**c**) 3 × 3 basket weave textile; (**d**) Knitted biaxial textile ($\infty \times \infty$).

Figure 7 illustrates the dimensions of the layer model-cell and the identification markings on its side faces. Table 2 summarizes the geometric characteristics of the model-cells. The volume fraction φ_f of the textile in the composite layer is only slightly affected by the waviness of the fiber bundles. The fiber bundles are most wavy in the plain weave textile, where $\varphi_f = 0.461$. In knitted biaxial textiles, there are no under-and-over crossings. The volume fraction of the textile is $\varphi_f = 0.459$. The difference is only 0.2%, so it does not significantly affect the macroscopic material properties of the composite layer.

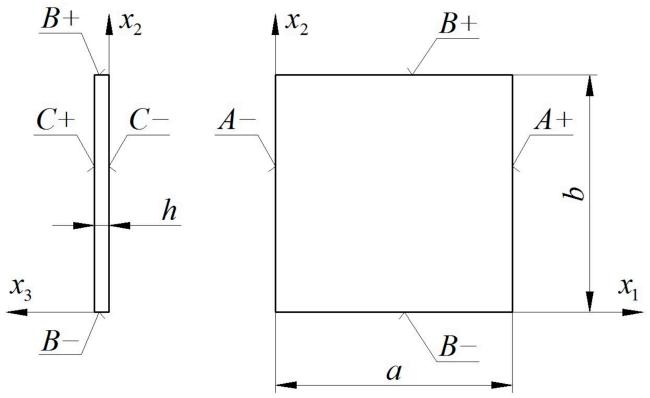


Figure 7. Dimensions and side faces of the layer model-cell.

Table 2. Geometric characteristics of the model-cells.

(a)	1 × 1	$a = b = 4$ mm	$V = 4$ mm^3	$\varphi_f = 0.461$	$\varphi_m = 0.539$	$h = 0.25$ mm
(b)	2 × 2	$a = b = 8$ mm	$V = 16$ mm^3	$\varphi_f = 0.460$	$\varphi_m = 0.540$	
(c)	3 × 3	$a = b = 12$ mm	$V = 36$ mm^3	$\varphi_f = 0.460$	$\varphi_m = 0.540$	
(d)	∞ × ∞	$a = b = 4$ mm	$V = 4$ mm^3	$\varphi_f = 0.459$	$\varphi_m = 0.541$	

4.2. Finite Element Modeling

I performed the finite element computation using NX I-deas 6.1 software. Each model-cell was meshed using quadratic tetrahedral elements of uniform size. The 3×3 basket weave structure has the largest repeating weave unit. Its finite element mesh is shown in Figure 8a. The warp rovings are represented by blue elements, while the weft rovings are represented by green elements. Figure 9 shows the meshed layer model-cell with plain weave textile reinforcement. The red elements mark the matrix. The XYZ coordinate system shown in Figures 8a and 9 corresponds to the $x_1x_2x_3$ coordinate system of Figures 7 and 8b.

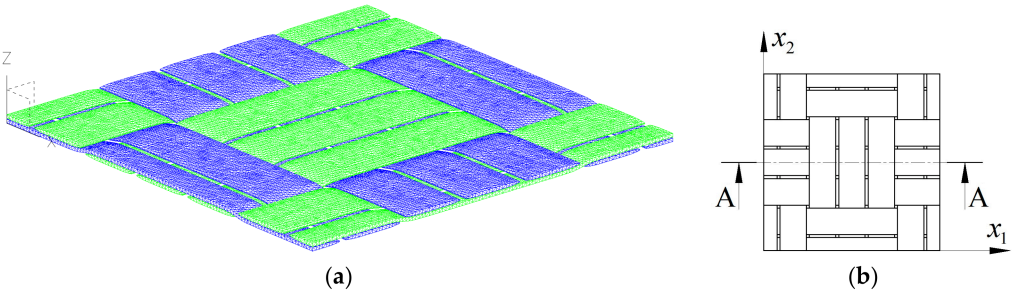


Figure 8. 3 × 3 basket weave textile: (**a**) Finite element mesh; (**b**) Cutting plane A−A of the textile.

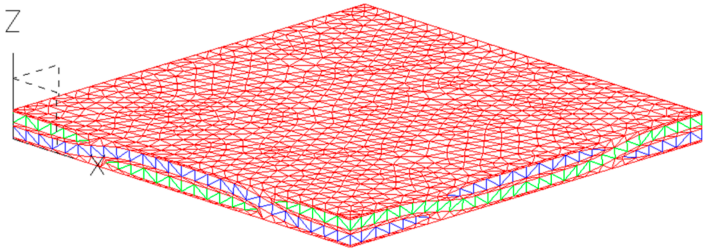


Figure 9. Layer model-cell reinforced with plain weave textile. Red: matrix, blue: warp rovings, green: weft rovings.

The textile reinforcement is identical in the x_1 and x_2 directions. Therefore, $E_1 = E_2$ and $\nu_{12} = \nu_{21}$ in Equation (1). To determine the material properties of the composite layer, two loading cases were analyzed for each model-cell: uniaxial tension in the x_1 direction to compute E_1, E_2, ν_{12}, ν_{21}, and shear in the x_1x_2 plane to determine the shear modulus G_{12}. I performed the finite element analyses following the procedure described by me et al. [10]. Periodic boundary conditions were applied to the nodes, and kinematic loading was prescribed through the nodal displacement field. The average stress $\overline{\sigma}_{ij}$ in Equation (3), was calculated from the reaction forces acting on the side faces.

5. Results

Table 3 summarizes the material properties calculated for four model-cells reinforced with different textile architectures. The numerical simulations indicate that reducing the number of fiber-bundle undulations within a given length increases the E_1 elastic modulus

of the composite layer while decreasing its ν_{12} Poisson's ratio. This trend can be observed in Figure 10. The calculated E_1 and ν_{12} material properties were plotted as a bar chart against the number of $p \times q$ fiber-bundle crossings. As shown in Table 3, the number of under-and-over crossings of rovings has no effect on the G_{12} shear modulus of the composite layer.

Table 3. Material properties calculated using the layer model-cell.

	$p \times q$	Specified Material Properties		
(a)	1×1	$E_1 = E_2 = 50{,}720$ MPa	$\nu_{12} = \nu_{12} = 0.103$	$G_{12} = 2900$ MPa
(b)	2×2	$E_1 = E_2 = 53{,}750$ MPa	$\nu_{12} = \nu_{12} = 0.060$	$G_{12} = 2900$ MPa
(c)	3×3	$E_1 = E_2 = 54{,}885$ MPa	$\nu_{12} = \nu_{12} = 0.047$	$G_{12} = 2900$ MPa
(d)	$\infty \times \infty$	$E_1 = E_2 = 57{,}850$ MPa	$\nu_{12} = \nu_{12} = 0.031$	$G_{12} = 2900$ MPa

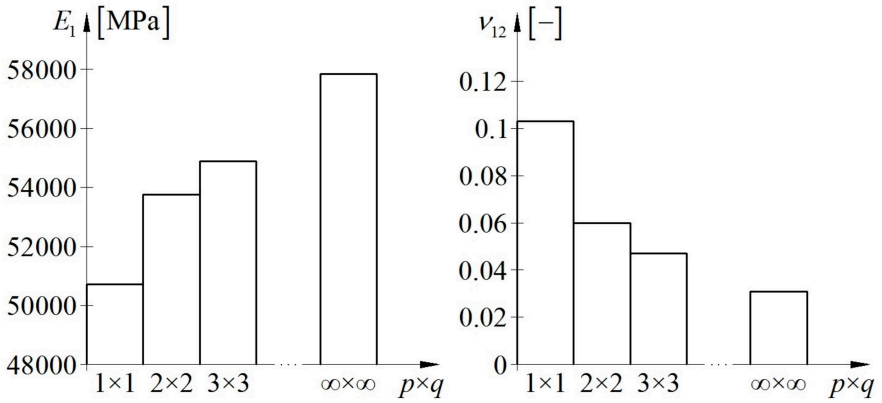


Figure 10. Variation of E_1 and ν_{12} as a function of $p \times q$.

The angle α_{r1}^{max} in Figure 5 decreases in the warp rovings under x_1 directional tension, resulting in a greater elongation of the composite layer. The angle α_{r1}^{max} increases in the weft rovings, thereby increasing transverse contraction. In the $x_{r1}x_{r2}x_{r3}$ material coordinate system, this results from the shear of the fiber bundles in the $x_{r1}x_{r3}$ plane and their bending along the x_{r2} axis. I analyzed the stresses in the homogenized fiber bundles and the matrix. The homogenized stress distributions in the 3×3 basket weave textile are shown in the cutting plane A−A indicated in Figure 8b. Figure 11 shows the $\overline{\tau}_{r13}$ homogenized shear stress distribution under x_1 directional tension with prescribed $\bar{\varepsilon}_1 = 2 \cdot 10^{-3}$ kinematic loading. The maximum absolute shear stress occurs near the inflection point of the weave. Figure 12 shows the $\overline{\sigma}_{r1}$ homogenized stress distribution in the cutting plane A−A of the central warp roving. Examining the difference in $\overline{\sigma}_{r1}$ stress between the lower and upper fibers, it can be seen that bending about the x_{r2} axis occurs before and after the inflection point of the weave.

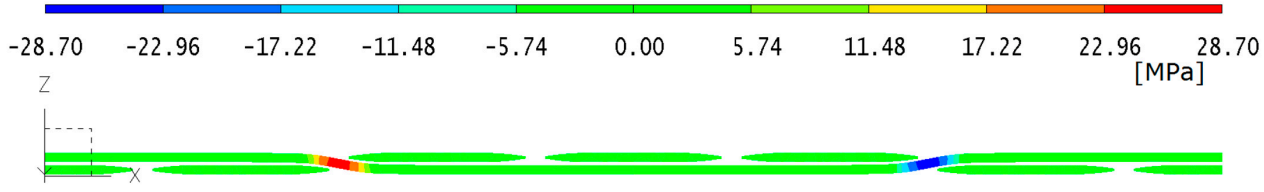


Figure 11. $\overline{\tau}_{r13}$ homogenized stress distribution in the A−A cutting plane of the textile.

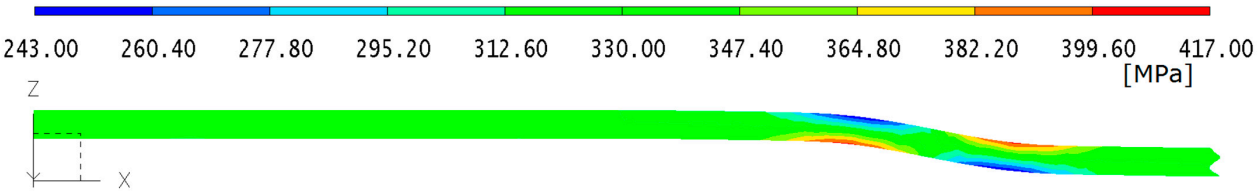


Figure 12. $\overline{\sigma}_{r1}$ homogenized stress distribution in the A−A cutting plane of the central warp roving.

There is no significant bending or shear in the straight sections of the fiber bundles. Therefore, increasing the number of fiber bundles $(p \times q)$ increases the stiffness of the composite layer in the x_1 and x_2 directions and reduces transverse contraction.

Figure 13 shows the τ_{12} shear stress distribution on the $A+$ side surface of a composite layer reinforced with a 3 × 3 basket weave textile during a shear test in the x_1x_2 plane. The prescribed kinematic loading was $\overline{\gamma}_{12} = 2 \cdot 10^{-3}$. The $A+$ side is shown in Figure 7. When comparing locations A, B, and C, the τ_{12} stress distribution at the under-and-over crossings is nearly the same as in regions where the fiber bundles run straight. The number of fiber bundles $(p \times q)$ does not affect the homogenized $\overline{\tau}_{12}$ shear stress on the side faces and the G_{12} shear modulus of the composite layer.

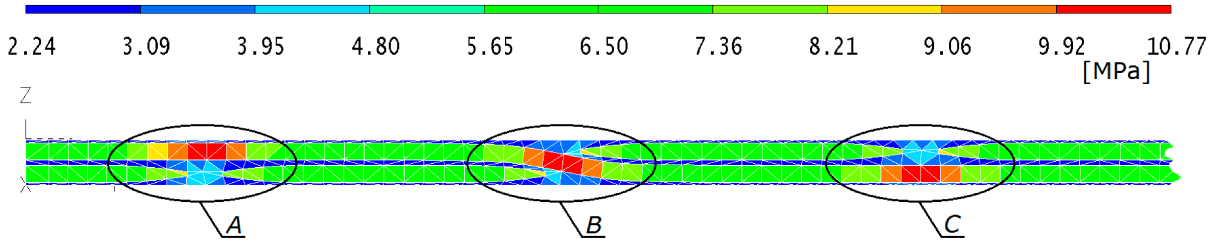


Figure 13. τ_{12} stress distribution on the $A+$ side face during the shear test in the x_1x_2 plane.

6. Conclusions

I determined the effect of changes in the textile weave pattern on the material properties of the composite layer using a layer model-cell and parametric analysis.

The results demonstrate that reducing the number of weave-induced undulations over a given length increases the moduli of elasticity of the composite layer in warp and weft directions, while reducing transverse contraction. It was also found that the shear modulus is not affected by the weave pattern.

Funding: This research received no external funding.

Institutional Review Board Statement: Not applicable.

Informed Consent Statement: Not applicable.

Data Availability Statement: The data published in this research are available on request from the author.

Conflicts of Interest: The author declare no conflict of interest.

References

1. Li, Y.; Dai, X.-Q. *Biomechanical Engineering of Textiles and Clothing*; CRC Press: Boca Raton, FL, USA, 2006.
2. Balaguru, P.N.; Wayne, K.L. Construction of Fiber Reinforced Polymer (FRP) Jackets for the Protection of Pier Caps. Construction Report. 2005. Available online: https://cait.rutgers.edu/wp-content/uploads/2018/05/ri-ru6862_0.pdf (accessed on 23 January 2026).
3. Barbero, E.J. *Finite Element Analysis of Composite Materials Using Ansys*; CRC Press: Boca Raton, FL, USA, 2014.
4. Bojtár, G. The Effect of Ratio of Fiber bundles in the Textile Composite Layer. *J. Mech. Eng.* **2024**, *74*, 1–10. [CrossRef]

5. Kollár, L.P.; Springer, G.S. *Mechanics of Composite Structures*; Cambridge University Press: Cambridge, UK, 2003.
6. Leijan, H. Determining Micro- and Macro- Geometry of Fabric and Fabric Reinforced Composites. Ph.D. Thesis, Department of Mechanical and Nuclear Engineering College of Engineering, Kansas State University, Manhattan, KS, USA, 2013.
7. Bhaskara, S.; Devireddy, R.; Biswas, S. Effect of Fiber Geometry and Representative Volume Element on Elastic and Thermal Properties of Unidirectional Fiber-Reinforced Composites. *Hindawi Publ. Corp. J. Compos.* **2014**, *629175*, 1–12. [CrossRef]
8. Xia, Z.; Zhang, Y.; Ellyin, F. A Unified Periodical Boundary Conditions for Representative Volume Elements of Composites and Applications. *Int. J. Solids Struct.* **2003**, *40*, 1907–1921. [CrossRef]
9. Bunsell, A.R.; Renard, J. *Fundamentals of Fibre Reinforced Composite Materials*; Series in Material Science and Engineering; CRC Press: Boca Raton, FL, USA, 2005.
10. Bojtár, G.M.; Csizmadia, B.; Égert, J. Numerical Determination of Orthotropic Material Properties of Textile Composite Layers and their Validation by Measurement. *Acta Polytech. Hung.* **2017**, *14*, 47–67. [CrossRef]
11. Bojtár, G.M.; Csizmadia, B.; Égert, J. Numerical Estimation Method of Orthotropic Material Properties of a Roving for Reinforcement of Composite Materials. *Acta Polytech. Hung.* **2016**, *13*, 163–182. [CrossRef]
12. *ASTM D638-10*; Standard Test Method for Tensile Properties of Plastics. ASTM: West Conshohocken, PA, USA, 2010.

Disclaimer/Publisher's Note: The statements, opinions and data contained in all publications are solely those of the individual author(s) and contributor(s) and not of MDPI and/or the editor(s). MDPI and/or the editor(s) disclaim responsibility for any injury to people or property resulting from any ideas, methods, instructions or products referred to in the content.